

Laser-induced rotation of iodine molecules in He-nanodroplets: revivals and breaking-free

Benjamin Shepperson,¹ Anders A. Søndergaard,² Lars Christiansen,¹ Jan Kaczmarczyk,³ Robert E. Zillich,^{4,*} Mikhail Lemeshko,^{3,†} and Henrik Stapelfeldt^{1,‡}

¹*Department of Chemistry, Aarhus University, 8000 Aarhus C, Denmark*

²*Department of Physics and Astronomy, Aarhus University, 8000 Aarhus C, Denmark*

³*IST Austria (Institute of Science and Technology Austria), Am Campus 1, 3400 Klosterneuburg, Austria*

⁴*Institute for Theoretical Physics, Johannes Kepler Universität Linz, Altenbergerstraße 69, A-4040 Linz, Austria*

(Dated: February 25, 2022)

Rotation of molecules embedded in He nanodroplets is explored by a combination of fs laser-induced alignment experiments and angulon quasiparticle theory. We demonstrate that at low fluence of the fs alignment pulse, the molecule and its solvation shell can be set into coherent collective rotation lasting long enough to form revivals. With increasing fluence, however, the revivals disappear – instead, rotational dynamics as rapid as for an isolated molecule is observed during the first few picoseconds. Classical calculations trace this phenomenon to transient decoupling of the molecule from its He shell. Our results open novel opportunities for studying non-equilibrium solute-solvent dynamics and quantum thermalization.

Usually, molecules dissolved in a liquid are not rotating freely due to the intermolecular forces exerted by the surrounding solvent. An important exception is molecules embedded in liquid helium nanodroplets where high-resolution infrared [1] and microwave [2] spectroscopies display discrete rotational structure. These observations along with theoretical modelling has established a picture that molecules inside He nanodroplets can rotate frictionless although followed by a local solvation shell of He atoms. This shell increases the effective molecular moment of inertia compared to the gas-phase value [3, 4].

These unique properties build the expectation that it should be possible to induce frictionless rotation of molecules inside Helium droplets and follow it in real time. For isolated molecules versatile techniques based on moderately intense fs or ps laser pulses have been developed to control the rotational degrees of freedom [5–7]. In particular, such methods have been extensively used to confine molecular axes to laboratory-fixed axes – methods referred to as alignment and orientation [5]. Recently, the first time-resolved experiments of molecular rotation inside He droplets revealed that moderately intense laser pulses can induce alignment of molecules [8, 9]. The measurements showed, however, no sign of frictionless rotation. Notably, the transient alignment-recurrences (revivals) characteristic of freely rotating molecules in gas phase were absent. These observations seemed at odds with the prevailing conception of rotational structure obtained through spectroscopy [3, 4].

Here we experimentally demonstrate that a sufficiently weak fs pulse can initiate coherent rotation of iodine molecules together with their He solvation shell – lasting long enough to form revivals. Our observations are rationalized by a quantum theory based on the angulon quasiparticle [10–15]. For strong alignment pulses the revivals disappear and, instead, strikingly fast rotational

dynamics appears immediately after the pulse. Classical estimates indicate that, in this regime, He atoms of the solvation shell detach from the molecule due to the centrifugal force generated by the rapid rotation. This can be seen as a sudden decoupling of the molecule from its solvent and for a short time the rotational motion resembles that of a free molecule.

In our experiment, 10-nm-diameter helium droplets – each doped with at most one iodine (I_2) molecule – are first irradiated by a 450 fs linearly polarized laser pulse at 800 nm. The purpose of this kick pulse is to induce alignment of the molecules, i.e. confine their I–I internuclear axis along the polarization direction [5]. Next, the molecules are Coulomb exploded by a delayed, intense probe pulse (40 fs, 3.7×10^{14} W/cm²) which produces IHe^+ ion fragments with recoil directions given by the angular distribution of the molecular axes at the instant of the probe pulse. By detecting the emission directions of the IHe^+ ions with a 2D imaging detector at many different kick-probe delays, t , the time-dependent degree of alignment, $\langle \cos^2 \theta_{2D} \rangle$, can be determined – θ_{2D} being the angle between the alignment pulse polarization and the projection of an IHe^+ ion velocity vector on the detector [16]. More details on the experimental setup are provided in the Supplemental Material [17].

Figure 1 shows $\langle \cos^2 \theta_{2D} \rangle$ as a function of time for a series of different fluences of the kick pulse, F_{kick} . At low F_{kick} there is a distinct maximum in $\langle \cos^2 \theta_{2D} \rangle$ shortly after the kick pulse [Fig. 1(a)-(d)]. The prompt peak grows in amplitude and appears earlier as F_{kick} is increased [Fig. 1(a2)-(d2)]. This behavior is the result of faster rotation and more efficient alignment induced by a stronger kick pulse and appears similar to previous measurements on CH_3I molecules in He droplets [8]. The current data exhibit, however, new, previously unobserved features. First, at $F_{\text{kick}} = 1.2$ J/cm² the prompt alignment peak is followed by pronounced yet decreasing

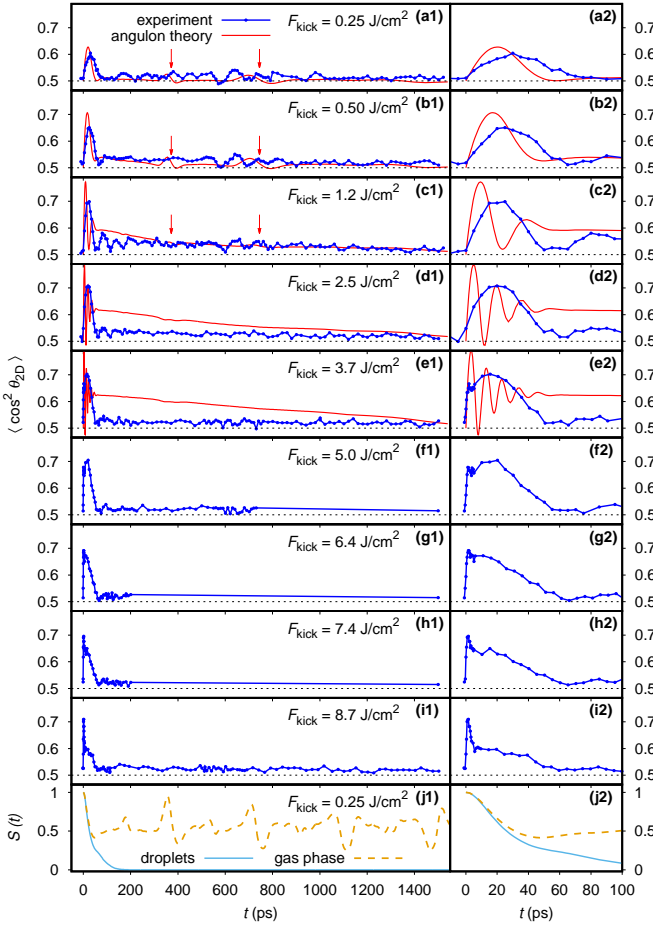


Figure 1. The degree of alignment, $\langle \cos^2 \theta_{2D} \rangle$, as a function of time at different fluences of the kick pulse (centered at $t = 0$); blue curves: experimental results, red curves: results from the angulon theory. In panel (f1) the time-interval 750–1500 ps and in panels (g1) and (h1) the time-interval 200–1500 ps are shown as straight lines because, for experimental reasons, $\langle \cos^2 \theta_{2D} \rangle$ was not recorded in these regions. The right column of panels expands on the first 100 ps to highlight the structure that starts to appear at $F_{\text{kick}} = 3.7 \text{ J/cm}^2$ immediately after the kick pulse and grows to a sharp peak with maximum at $t = 1.3 \text{ ps}$ for $F_{\text{kick}} = 8.7 \text{ J/cm}^2$. Panels (j) show the survival probability of the initial state, as defined in the text.

oscillations out to $\sim 200 \text{ ps}$. Second, for $F_{\text{kick}} = 0.25, 0.50$ and 1.2 J/cm^2 an oscillatory structure is observed in the interval 550–750 ps. The structure is very similar for the three fluences with local maxima and minima at essentially the same times. Third, on average the $\langle \cos^2 \theta_{2D} \rangle$ curves are gradually decaying in the range ~ 100 –1500 ps for $F_{\text{kick}} = 0.50, 1.2$ and 2.5 J/cm^2 .

For $F_{\text{kick}} \geq 2.5 \text{ J/cm}^2$ the structure in the 550–750 ps interval disappears. Also, the oscillations after the main peak are strongly reduced for $F_{\text{kick}} = 2.5 \text{ J/cm}^2$ and essentially absent at larger fluences. Instead a substructure in the prompt alignment peak starts to appear at $F_{\text{kick}} = 3.7 \text{ J/cm}^2$ [Fig. 1(e2)]. As the fluence is increased the

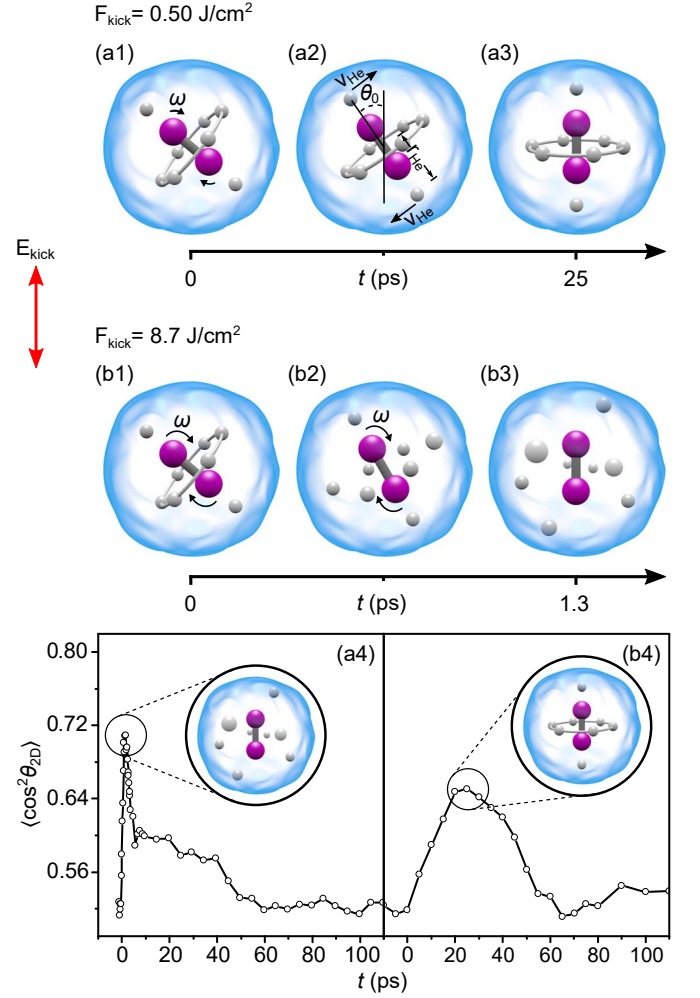


Figure 2. Schematic illustration of laser-induced rotation of I_2 molecules inside He droplets, based on the classical model described in the text, for a weak [(a1)–(a3)] and a strong [(b1)–(b3)] kick pulse. (a4) and (b4) relate the illustrations to the data recorded. (a2) illustrates parameters used in the classical model. θ_0 : The angle between the molecular axis and the kick pulse polarization just prior to the laser-molecule interaction. r_{He} : Distance from the He atom at the ends to the axis of rotation. v_{He} : The linear speed of the He atoms at the ends of the molecule gained from the laser-molecule interaction.

substructure grows to a prominent sharp peak ending with a maximum already at $t \sim 1.3 \text{ ps}$ for $F_{\text{kick}} = 8.7 \text{ J/cm}^2$ [Figs. 1(i) and 4].

We interpret the oscillations after the prompt peak and the 550–750 ps structure as manifestations of coherent rotation of the molecules and their local He solvation shell — hereafter termed He-dressed molecules. To substantiate this interpretation we first model He-dressed molecules as classical rigid rotors driven by the polarizability interaction with the kick pulse. A He-dressed molecule initially at an angle θ_0 to the kick pulse polar-

ization [Fig. 2(a3)] gains an angular velocity, ω , of [18]:

$$\omega = \frac{1}{2} \frac{\Delta\alpha F_{\text{kick}} \sin(2\theta_0)}{I_{\text{eff}} \varepsilon_0 c}, \quad (1)$$

where $\Delta\alpha$ is the polarizability anisotropy of I_2 and I_{eff} is the effective moment of inertia of I_2 in the droplets. No experimental value exists for I_{eff} so we determined it by a path integral Monte Carlo calculation [19], which gave $I_{\text{eff}} = 1.7 \times I_0$ where I_0 is the moment of inertia of the bare I_2 molecule. The calculated He density around the I_2 molecule is shown in Fig. 3. In our classical calculations a He-dressed molecule is treated as an I_2 molecule rigidly attached to eight He atoms placed in the minima of the I_2 -He potential [1, 20] (six He atoms in the central ring around the molecule and two at the ends), see Fig. 2. The value of I_{eff} determined from this structure (Fig. 2) is essentially equal to the Monte Carlo one.

Equation (1) predicts that the He-dressed molecules are set into end-over-end rotation (Fig. 2) leading to a prompt alignment peak as observed experimentally. Continued rotation for extended times requires that superfluidity of the droplets is undistorted. A simple classical criterion for this is that the linear speed of the outer components of the He-dressed molecules should not exceed the Landau velocity, $v_L = 56$ m/s [21]. The highest linear speed is calculated as $v_{\text{He}} = \omega r_{\text{He}}$, where r_{He} is the distance from a He atom at the ends to the axis of rotation (see Fig. 2). Table I displays the values of ω and v_{He} for the nine different fluences used in the experiment. For $F_{\text{kick}} = 0.25$ and 0.50 J/cm² $v_{\text{He}} < v_L$, whereas at $F_{\text{kick}} = 1.2$ J/cm² v_{He} is just above v_L . At higher fluences, $v_{\text{He}} \gg v_L$ for almost all of the He-dressed molecules – independent of their initial orientation. These simple classical considerations indicate that long-time coherent rotational dynamics of the He-dressed molecules is only possible for the three lowest fluences – in accordance with the observations – and illustrated by panels (a1)-(a3) of Fig. 2.

To elucidate the quantum dynamics of the system, we apply the recently-developed angulon theory [10–15, 22, 41]. The angulon represents a quasiparticle consisting of a molecular rotor dressed by a many-body field of superfluid excitations, and can be thought of as a quantum formulation of the He-dressed molecule. Recently it was shown that molecules in superfluid helium form angulons [22]. The case of I_2 in helium belongs to the strong-coupling regime, where the molecular kinetic energy is small compared to the molecule-helium interactions [12, 22]. In this regime, the angulon theory furnishes a closed-form expression for the alignment

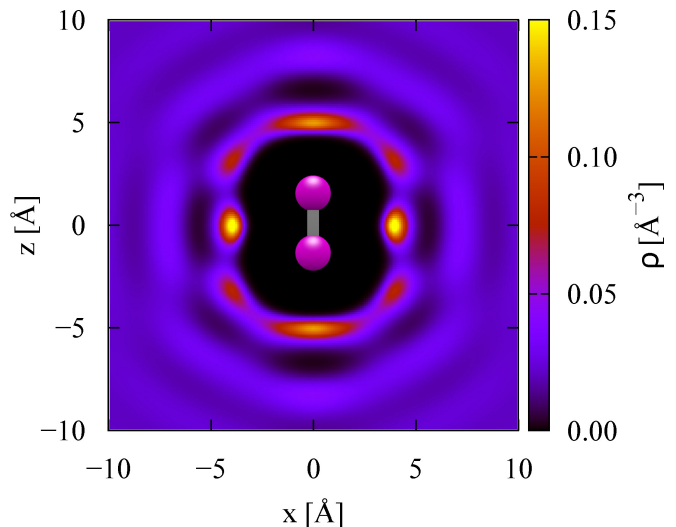


Figure 3. He density, ρ , around I_2 in the molecular frame in equilibrium. It is obtained from a path integral Monte Carlo calculation [17] and corresponds to the situation prior to the kick pulse.

cosine:

$$\begin{aligned} & \langle \cos^2 \hat{\theta}_{2D} \rangle(t) \\ &= \sum_{j,j',j_1,j_2,m} c_{j'}^* c_j e^{it(E_{j_2} + E_{j'} - E_{j_1} - E_j)/2} \langle j_2 m | \cos^2 \hat{\theta}_{2D} | j_1 m \rangle \\ & \times \int d\Omega_1 \int d\Omega_2 Y_{j'm_0}^*(\Omega_2) Y_{j_2 m}(\Omega_2) Y_{j m_0}(\Omega_1) Y_{j_1 m}^*(\Omega_1) \\ & \times e^{\alpha_1 t^2 [\frac{4\pi}{5} \sum_{\mu} Y_{2,\mu}(\Omega_2) Y_{2,\mu}^*(\Omega_1) - 1]}. \quad (2) \end{aligned}$$

(in units of $\hbar \equiv 1$). Here $E_j = B_{\text{eff}} j(j+1)$ are the molecular rotational energies, with B_{eff} the effective rotational constant of I_2 . α_1 parametrizes the anisotropic molecule-helium interactions, with the strong-coupling regime defined by $B_{\text{eff}} \ll \sqrt{\alpha_1}$. The coefficients, $c_j = \langle j, m_0 | \exp(\eta \cos^2 \hat{\theta}) | j_0, m_0 \rangle$, describe the rotational wavepacket created from the initial molecular state $|j_0, m_0\rangle$ by a short laser pulse with a dimensionless intensity η . In order to compare the theory to experiment, the results of Eq. (2) were averaged over the thermal distribution of the initial states and the finite width of rotational lines due to dephasing was accounted for. More details on the theoretical approach are provided in the Supplemental Material [17].

The strong-coupling angulon theory is straightforward to apply if the molecule-laser interaction energy $\eta \lesssim \sqrt{\alpha_1}$. This is the case in Fig. 1 (a) and (b), where $\eta/\sqrt{\alpha_1} \approx 1.4$ and 2.7, respectively. Both calculated $\langle \cos^2 \theta_{2D} \rangle$ curves (red) are dominated by a prominent peak at early times. For $F_{\text{kick}} = 0.25$ and 0.50 J/cm² the prompt alignment peak agrees with the experimental curves although the peak amplitude is somewhat higher for the calculated curves. We ascribe this to an underestimation of the

$F_{\text{kick}}, \text{J/cm}^2$	$\omega, 10^{10} \text{ Hz}$	$v_{\text{He}}, \text{m/s}$	$E_{\text{rot}}(\text{He}), \text{cm}^{-1}$
0.25	2.7	13	0.029
0.50	5.5	26	0.12
1.2	14	65	0.71
2.5	27	130	2.8
3.7	41	195	6.4
5.0	54	260	11
6.4	70	338	19
7.4	81	390	26
8.7	95	454	35

Table I. Classical calculation of the maximum angular velocity using Eq. (1) with $\theta_0 = 45^\circ$ for the nine different fluences used in the experiment. From ω the linear speed, v_{He} , and the rotational energy, $E_{\text{rot}}(\text{He})$, of the He atoms at the ends of the molecules are calculated – see text.

measured degree of alignment due to non-axial recoil effects in the Coulomb explosion process, caused by the He environment [23]. The fluence of $F_{\text{kick}} = 1.2 \text{ J/cm}^2$ corresponds to $\eta/\sqrt{\alpha_1} \approx 7$ and therefore lies beyond the reach of the strong-coupling angulon theory which predicts a faster initial dynamics compared to the experiment. Nevertheless, the long-time decay of alignment observed experimentally is reproduced. For higher fluences, $F_{\text{kick}} = 2.5 \text{ J/cm}^2$ and $F_{\text{kick}} = 3.7 \text{ J/cm}^2$, the molecule-laser interactions dominate over molecule-helium interactions, since $\eta/\sqrt{\alpha_1} \approx 14$ and 21, respectively.

For $F_{\text{kick}} = 0.25$ and 0.50 J/cm^2 low-amplitude structures just before 400 and 800 ps are visible. The angulon model identifies these as the half- and full-revival of the He-dressed molecule, marked by red arrows for the theoretical curves. The locations of the revival structures match $\hbar/(4B_{\text{eff}})$ and $\hbar/(2B_{\text{eff}})$, with $B_{\text{eff}} = \hbar^2/(2I_{\text{eff}})$, similar to the well-studied case of isolated molecules. The magnitude of the revivals decreases for larger fluences, and they are no longer visible for $F_{\text{kick}} \geq 2.5 \text{ J/cm}^2$.

Importantly, the angulon theory predicts that rotational revivals are possible for molecules strongly interacting with superfluid helium. Therefore, we interpret the observed oscillatory structure in the 550–750 ps interval as a full rotational revival of the He-dressed molecule. Furthermore, we note that the model captures the overall decay of $\langle \cos^2 \theta_{2D} \rangle$ observed most clearly for $F_{\text{kick}} = 0.50$ and 1.2 J/cm^2 . We quantify this decay by the survival probability (closely related to the Loschmidt echo [24]), $S(t) = |\langle \psi(t) | \psi_0 \rangle|^2 \equiv |\langle \psi_0 | e^{iHt} | \psi_0 \rangle|^2$, of the state $|\psi_0\rangle$ immediately after the kick pulse excitation during time evolution under the angulon Hamiltonian H [17]. The time-dependence of the survival probability is shown in Fig. 1j. While the gas-phase survival probability (dashed line) exhibits revivals similar to the gas-phase molecular alignment, for I_2 in helium we predict a Gaussian decay $S(t) \sim \exp(-\alpha_1 t^2)$ [17]. The latter comes from redistribution of the angular momentum between the molecule and the superfluid. Note that this decay occurs on a faster timescale compared to the ex-

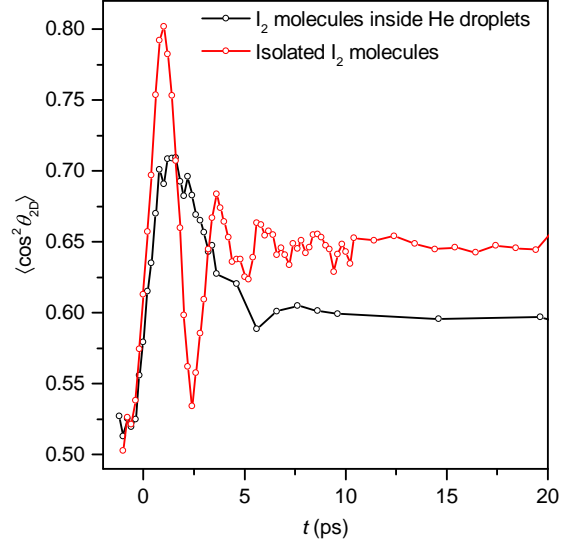


Figure 4. The degree alignment, $\langle \cos^2 \theta_{2D} \rangle$, at early times for isolated I_2 molecules and I_2 molecules in He droplets recorded for $F_{\text{kick}} = 8.7 \text{ J/cm}^2$. The laser parameters of both the kick pulse and the probe pulse were identical for the measurements on the isolated molecules and on the molecules in He droplets.

ponential decay common for Markovian reservoirs [25].

In the high-fluence regime, $\eta/\sqrt{\alpha_1} \gg 1$, the strong-coupling angulon theory is not applicable. However, classically, a high-fluence pulse can induce such a fast rotation of the He-dressed molecule that helium atoms detach due to the centrifugal force – a mechanism which, we believe, is responsible for the sharp structure appearing in the prompt alignment peak. A simple criterion for detaching one He atom is: $E_{\text{rot}}(\text{He}) > E_{\text{binding}}(\text{He})$, where $E_{\text{rot}}(\text{He}) = \frac{1}{2} m_{\text{He}} r_{\text{He}}^2 \omega^2$ is the rotational energy of a He atom and $E_{\text{binding}}(\text{He}) \approx 16 \text{ cm}^{-1}$ is the ground-state binding energy of the HeI_2 complex [20, 26]. Table I displays $E_{\text{rot}}(\text{He})$ calculated for the different fluences. At $F_{\text{kick}} \gtrsim 6 \text{ J/cm}^2$ the criterion is met implying that one or indeed several He atoms detach from the molecule (lower panels in Fig. 2) since the binding energies of the first few He atoms are similar [27].

Figure 4 compares the short-time alignment dynamics of molecules in He droplets to that of isolated molecules at $F_{\text{kick}} = 8.7 \text{ J/cm}^2$. In droplets, $\langle \cos^2 \theta_{2D} \rangle$ evolves almost as fast as $\langle \cos^2 \theta_{2D} \rangle$ of isolated molecules during the first ~ 2 ps. In classical terms, this indicates that I_2 rotates almost freely, detached from the He atoms. We observed the same rapid short-time alignment dynamics for OCS and CS_2 molecules in He droplets. At $t > 2$ ps the free rotation is quenched, which indicates a dynamical re-formation of the He-dressed molecule.

Our results demonstrate that for molecules embedded

in He droplets a moderately intense laser pulse can induce coherent collective rotation of a molecule and its solvation shell for times long enough to form rotational revivals. These findings reconcile femtosecond laser-induced molecular alignment and high-resolution infrared and microwave spectroscopy. Our angulon quasiparticle theory rationalizes the observations for the low-fluence experimental results. Future generalization of the theory may lead to a quantitative agreement with experiments in a broad range of laser fluences and is expected to provide new insights into the superfluid behavior of He droplets. Finally, the observed decoupling of the molecule from its He-solvation shell at high fluences draws parallels to the nonlinear response in the solute-solvent interaction of rapidly rotating CN molecules dissolved in ethanol [28, 29]. Our results open unique opportunities for real-time studies of non-equilibrium solute-solvent dynamics, for instance, by gradually modifying the solvation shell through insertion of other noble gas atoms or even water molecules [4]. Furthermore, experiments on molecules in small helium droplets might yield insight into quantum thermalization of finite many-particle systems [30, 31].

We thank Richard Schmidt for insightful discussions. JK acknowledges support from People Programme (Marie Curie Actions) of the European Union's Seventh Framework Programme (FP7/2007-2013) under REA grant agreement No. [291734]. REZ acknowledges support from the Austrian Science Fund (FWF) under grant No. P23535-N20. ML acknowledges support from the Austrian Science Foundation (FWF), under grant No. P29902-N27. HS acknowledges support from the European Research Council-AdG (Project No. 320459, DropletControl) and the Villum Foundation.

* Corresponding author: Robert.Zillich@jku.at

† Corresponding author: mikhail.lemeshko@ist.ac.at

‡ Corresponding author: henriks@chem.au.dk

- [1] S. Grebenev, M. Hartmann, M. Havenith, B. Sartakov, J. P. Toennies, and A. F. Vilesov, *J. Chem. Phys.* **112**, 4485 (2000).
- [2] R. Lehnig, P. L. Raston, and W. Jäger, *Faraday Discuss.* **142**, 297 (2009).
- [3] J. P. Toennies and A. F. Vilesov, *Angew. Chem. Int. Ed.* **43**, 2622 (2004).
- [4] M. Y. Choi, G. E. Douberly, T. M. Falconer, W. K. Lewis, C. M. Lindsay, J. M. Merritt, P. L. Stiles, and R. E. Miller, *Int. Rev. Phys. Chem.* **25**, 15 (2006).
- [5] H. Stapelfeldt and T. Seideman, *Rev. Mod. Phys.* **75**, 543 (2003).
- [6] Y. Ohshima and H. Hasegawa, *Int. Rev. Phys. Chem.* **29**, 619 (2010).
- [7] A. Korobenko, A. A. Milner, J. W. Hepburn, and V. Milner, *Phys. Chem. Chem. Phys.* **16**, 4071 (2014).
- [8] D. Pentlehner, J. H. Nielsen, A. Slenczka, K. Mølmer, and H. Stapelfeldt, *Phys. Rev. Lett.* **110**, 093002 (2013).
- [9] L. Christiansen, J. H. Nielsen, D. Pentlehner, J. G. Underwood, and H. Stapelfeldt, *Phys. Rev. A* **92**, 053415 (2015).
- [10] R. Schmidt and M. Lemeshko, *Phys. Rev. Lett.* **114**, 203001 (2015).
- [11] M. Lemeshko and R. Schmidt, "Molecular impurities interacting with a many-particle environment: from ultracold gases to helium nanodroplets," in *Low Energy and Low Temperature Molecular Scattering*, edited by A. Osterwalder and O. Dulieu (RSC, 2017).
- [12] R. Schmidt and M. Lemeshko, *Phys. Rev. X* **6**, 011012 (2016).
- [13] E. Yakaboylu and M. Lemeshko, *Phys. Rev. Lett.* (in press); arXiv:1612.02820 (2017).
- [14] B. Midya, M. Tomza, R. Schmidt, and M. Lemeshko, *Phys. Rev. A* **94**, 041601(R) (2016).
- [15] X. Li, R. Seiringer, and M. Lemeshko, arXiv: 1610.04908 (2016).
- [16] A. Søndergaard, B. Shepperson, and H. Stapelfeldt, *J. Chem. Phys.* (in press) (2017).
- [17] See the Supplemental Material for details.
- [18] M. Leibscher, I. S. Averbukh, and H. Rabitz, *Phys. Rev. A* **69**, 013402 (2004).
- [19] R. E. Zillich, F. Paesani, Y. Kwon, and K. B. Whaley, *J. Chem. Phys.* **123**, 114301 (2005).
- [20] L. García-Gutierrez, L. Delgado-Tellez, Á. Valdés, R. Prosimi, P. Villarreal, and G. Delgado-Barrio, *J. Phys. Chem. A* **113**, 5754 (2009).
- [21] N. B. Brauer, S. Smolarek, E. Loginov, D. Mateo, A. Hernando, M. Pi, M. Barranco, W. J. Buma, and M. Drabbels, *Phys. Rev. Lett.* **111**, 153002 (2013).
- [22] M. Lemeshko, *Phys. Rev. Lett.* (in press); arXiv:1610.01604 (2017).
- [23] L. Christensen, L. Christiansen, B. Shepperson, and H. Stapelfeldt, *Phys. Rev. A* **94**, 023410 (2016).
- [24] P. R. Zangara, A. D. Dente, P. R. Levstein, and H. M. Pastawski, *Phys. Rev. A* **86**, 012322 (2012).
- [25] S. Ramakrishna and T. Seideman, *Phys. Rev. Lett.* **95**, 113001 (2005).
- [26] S. E. Ray, A. B. McCoy, J. J. Glennon, J. P. Darr, E. J. Fesser, J. R. Lancaster, and R. A. Loomis, *J. Chem. Phys.* **125**, 164314 (2006).
- [27] F. Paesani and K. B. Whaley, *J. Chem. Phys.* **121**, 4180 (2004).
- [28] A. C. Moskun, A. E. Jailaubekov, S. E. Bradforth, G. Tao, and R. M. Stratt, *Science* **311**, 1907 (2006).
- [29] G. Tao and R. M. Stratt, *J. Chem. Phys.* **125**, 114501 (2006).
- [30] M. Rigol, V. Dunjko, and M. Olshanii, *Nature* **452**, 854 (2008).
- [31] A. Polkovnikov, K. Sengupta, A. Silva, and M. Vengalattore, *Rev. Mod. Phys.* **83**, 863 (2011).
- [32] T. Seideman and E. Hamilton, *Adv. At. Mol. Opt. Phys.* **52**, 289 (2005).
- [33] D. Pentlehner, J. H. Nielsen, L. Christiansen, A. Slenczka, and H. Stapelfeldt, *Phys. Rev. A* **87**, 063401 (2013).
- [34] R. P. Feynman and A. R. Hibbs, *Quantum Mechanics and Path Integrals*, International Series in Pure and Applied Physics (McGraw-Hill, 1965).
- [35] D. Chandler and P. G. Wolynes, *J. Comp. Phys.* **74**, 4078 (1981).
- [36] D. M. Ceperley, *Rev. Mod. Phys.* **67**, 279 (1995).

- [37] M. Boninsegni, N. V. Prokofev, and B. V. Svistunov, Phys. Rev. E **74**, 036701 (2006).
- [38] R. A. Aziz, F. R. W. McCourt, and C. C. K. Wong, Mol. Phys. **61**, 1487 (1987).
- [39] N. Metropolis, A. W. Rosenbluth, M. N. Rosenbluth, A. H. Teller, and E. W. Teller, J. Chem. Phys. **21**, 1087 (1953).
- [40] N. Blinov, X. Song, and P.-N. Roy, J. Chem. Phys. **120**, 5916 (2004).
- [41] E. S. Redchenko and M. Leshenko, Chem. Phys. Chem. **17**, 3649 (2016).
- [42] D. A. Varshalovich, A. Moskalev, and V. Khersonskii, *Quantum theory of angular momentum* (World Scientific, 1988).
- [43] J. T. Devreese, arXiv:1012.4576 (2015).
- [44] A. Leggett, S. Chakravarty, A. T. Dorsey, M. P. A. Fisher, A. Garg, and W. Zwerger, Rev. Mod. Phys. **59**, 1 (1987).
- [45] R. Machleidt and D. Entem, Phys. Rep. **503**, 1 (2011).
- [46] E. Fradkin, *Field theories of condensed matter physics*, 2nd ed. (Cambridge University Press, 2013).
- [47] H. Lefebvre-Brion and R. W. Field, *The Spectra and Dynamics of Diatomic Molecules* (Elsevier, New York, 2004).
- [48] L. C. Biedenharn and J. D. Louck, *Angular momentum in quantum physics* (Addison-Wesley, 1981).
- [49] N. E. Henriksen, Chem. Phys. Lett. **312**, 196 (1999).
- [50] R. E. Zillich, K. B. Whaley, and K. von Haeften, J. Chem. Phys. **128**, 094303 (2008).

SUPPLEMENTAL MATERIAL

Experimental setup and method

A schematic diagram of the experimental setup used for laser-induced alignment experiments of iodine molecules, both solvated inside helium droplets and isolated in a supersonic beam, is shown in Fig. S1. Helium droplets are produced using a continuous helium droplet source with stagnation conditions of 14 K and 25 bar, giving ~ 10 nm diameter helium droplets [3]. Shortly after the exit of the continuous source the droplet beam passes through a

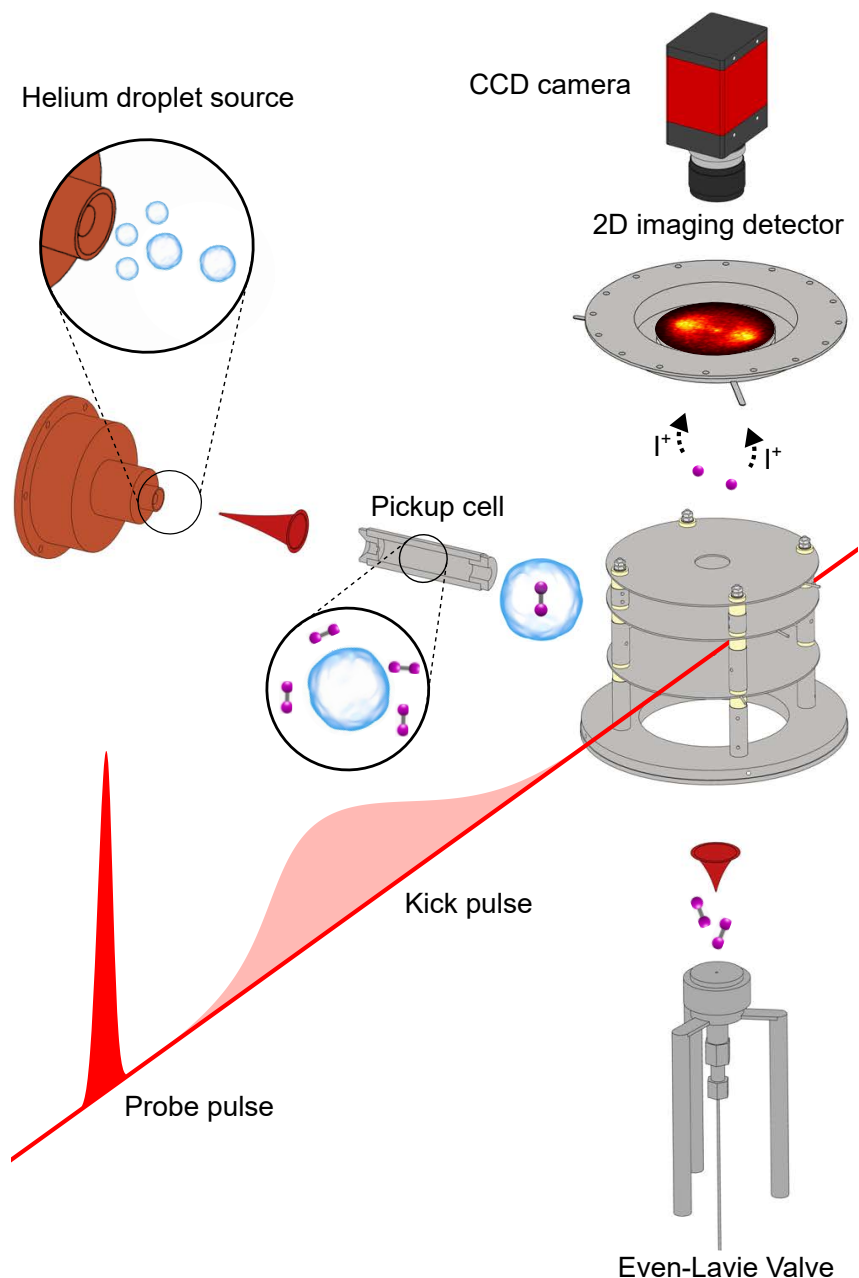


Figure S1. **Schematic of the experimental setup.** Schematic diagram showing the experimental setup used for the non-adiabatic alignment of iodine molecules both solvated inside helium droplets and isolated in a supersonic beam. Depicted from left to right are the continuous helium droplet source, the pickup cell and the 2D imaging spectrometer. Below the spectrometer sits the Even-Lavie pulsed valve used for the isolated molecule studies. The polarization state of the kick pulse (horizontal) and the delayed probe pulse (vertical) are indicated by the direction of the pulse forms sketched.

skimmer with a 1 mm diameter opening and enters a pickup cell containing iodine vapor. The partial pressure of the iodine vapor was kept sufficiently low to ensure the pickup of at most a single iodine molecule. Hereafter the doped droplets pass through a liquid nitrogen trap that captures the majority of the effusive iodine molecules that are not picked up by the droplets. In order to further reduce the contribution from effusive molecules the doped droplets pass through a second skimmer with a 2 mm diameter opening followed by a second liquid nitrogen trap. Finally, the doped droplets enter the interaction region of the target chamber. In this region, the doped helium droplet beam is crossed perpendicularly by two collinear 800 nm pulsed laser beams. The doped droplets are first irradiated with a linearly polarized kick pulse that is used to induce alignment. For the measurements up to $F_{\text{kick}} = 5.0 \text{ J/cm}^2$ the duration of the kick pulse is 450 fs. At this duration the fluence cannot be increased further because the intensity becomes so high that the iodine molecules starts to be ionized by the kick pulse alone. The measurements with $F_{\text{kick}} = 6.4, 7.4$ and 8.7 J/cm^2 are, therefore, recorded with a kick pulse duration of 1300 fs. This is still much shorter than the rotational time of the iodine molecule (446 ps in gas phase) and thus keeps the experiment in the strictly non-adiabatic limit of alignment [5, 32]. For consistency, we recorded the alignment experiment at $F_{\text{kick}} = 5.0 \text{ J/cm}^2$ with the 1300 fs kick pulse and got results essentially identical to those recorded with the 450 fs kick pulse (Fig. 1f in the main text).

After the kick pulse the molecules are Coulomb exploded by a delayed, intense probe pulse (40 fs, $3.7 \times 10^{14} \text{ W/cm}^2$), which produces I^+ or IHe^+ ion fragments. The recoil directions of either ion species are given by the angular distribution of the molecular axes at the instant of the probe pulse. For the measurements reported here the IHe^+ signal was chosen as the observable because these ions can only be produced from molecules inside He droplet [8, 33]. In the case of I^+ ions there is a contribution from those iodine molecules that manage to effuse from the pick-up cell to the interaction region in the target chamber. This contribution is, however, at most a few percent and recording of I^+ images could, therefore, also have been carried out and should give the same rotational dynamics as that obtained from the IHe^+ images.

By detecting the emission directions of the IHe^+ ions with a 2D imaging detector at many different kick-probe delays, t , the time-dependent degree of alignment, $\langle \cos^2 \theta_{2D} \rangle$, can be determined, where θ_{2D} is the angle between the kick pulse polarization and the projection of an IHe^+ ion velocity vector on the detector. The experimental setup is equipped with a pulsed Even-Lavie valve located beneath the target chamber and allows for a molecular beam of isolated iodine molecules to be sent into the interaction region. The alignment dynamics for isolated molecules was recorded under the same laser conditions as those used for the helium droplet experiments. Here I^+ ions were used as observables.

Path integral Monte Carlo

Quantum many-body systems of N particles in equilibrium can be mapped to a classical system of polymer chains [34, 35]. The path integral Monte Carlo (PIMC) method exploits this isomorphism. For Bose systems like ^4He droplets, finite-temperature results obtained by PIMC can be considered virtually exact, given sufficient simulation time.

The PIMC method calculates equilibrium properties in the canonical [36] or grand canonical [37] ensemble. In the present work we use the canonical ensemble, thus expectation values of an operator \hat{A} are obtained as $\langle \hat{A} \rangle = \frac{1}{Z} \text{Tr}[e^{-\beta \hat{H}} \hat{A}]$, where $Z = \text{Tr}[e^{-\beta \hat{H}}]$ is the partition function, $\beta = 1/k_B T$, and \hat{H} is the many-body Hamiltonian. In our case of a linear molecule with bare rotational constant B and mass M and N ^4He atoms of mass m \hat{H} is

$$\hat{H} = -\frac{\hbar^2}{2M} \nabla_0^2 + B \hat{L}^2 - \frac{\hbar^2}{2m} \sum_i \nabla_i^2 + \sum_i u(\mathbf{r}_0, \mathbf{r}_i, \Omega) + \sum_{i < j} v(|\mathbf{r}_i - \mathbf{r}_j|)$$

\hat{L} is the angular momentum operator, Ω are the two Euler angles of a linear molecule, \mathbf{r}_0 is the center of mass coordinate of the molecule and \mathbf{r}_i are the coordinates of the ^4He atoms. The interactions are modeled as pair-wise interactions between ^4He atoms, v , and between ^4He atoms and the molecule, u . We use the potential by Aziz et al. [38] for v and the *ab initio* potential by Garcia-Gutierrez et al. [20] for u . The latter depends not only on the distance $|\mathbf{r}_0 - \mathbf{r}_i|$ between ^4He atom and molecule, but also on the angle θ_i between the distance vector $\mathbf{r}_0 - \mathbf{r}_i$ and the axis of the molecule defined by Ω . It is the dependence on θ_i which leads to the coupling of the rotational dynamics of the molecule to the helium droplet. We neglect the vibrational degree of freedom of the molecule, which for a diatomic molecule like I_2 is the distance between the two iodine atoms. The vibrational excitation energies are orders of magnitude larger than typical rotational energies and excitation energies in helium. Therefore, the coupling

between vibrations and helium are negligible in the study of rotational dynamics. We assume I_2 to be a rigid rotor, with the two iodine atoms separated by their equilibrium distance of 2.666 Å.

For PIMC simulations, it is convenient to work in coordinate space. Thus, for calculating expectation values $\langle \hat{A} \rangle$ the many-body density matrix in configuration space, $\rho(\mathbf{R}, \mathbf{R}'; \beta) = \langle \mathbf{R} | e^{-\beta \hat{H}} | \mathbf{R}' \rangle$, is sampled using the Metropolis algorithm [39]. Here \mathbf{R} denotes all coordinates of the many-body system, $\mathbf{R} = (\Omega, \mathbf{r}_0, \mathbf{r}_1, \dots, \mathbf{r}_N)$. A numerical evaluation of $\rho(\mathbf{R}, \mathbf{R}'; \beta)$ is complicated by the fact that in general the exponential of the many-body Hamiltonian \hat{H} cannot be calculated. Therefore, we split the “imaginary time” interval β into small “time steps” $\tau = \beta/M$. This necessitates the introduction of new coordinates at intermediate time slices,

$$\rho(\mathbf{R}_0, \mathbf{R}_M; \beta) = \int d\mathbf{R}_1 \cdots d\mathbf{R}_{M-1} \rho(\mathbf{R}_0, \mathbf{R}_1; \tau) \cdots \rho(\mathbf{R}_{M-1}, \mathbf{R}_M; \tau). \quad (\text{S1})$$

$(\mathbf{R}_0, \dots, \mathbf{R}_M)$ can be regarded as a discretized path in imaginary time. This way each particle coordinate \mathbf{r}_i is replaced by a whole path of coordinates (“beads”) $\mathbf{r}_{i,j}$ where the new index $j = 0, \dots, M$ labels the discretized imaginary time.

For completing the isomorphism between a quantum system and classical polymers of beads, we choose τ sufficiently small, such that $\rho(\mathbf{R}_0, \mathbf{R}_1; \tau)$ can be approximated. We use the pair density approximation [36] for the He-He interaction, and the Trotter approximation for the He-molecule interaction, $e^{-\tau(\hat{T}+\hat{V})} = e^{-\tau\hat{V}/2} e^{-\tau\hat{T}} e^{-\tau\hat{V}/2} + \mathcal{O}(\tau^3)$, where \hat{T} and \hat{V} are the (non-commuting) kinetic and interaction terms of the Hamiltonian $\hat{H} = \hat{T} + \hat{V}$, respectively. The Trotter approximation requires to use a relatively small time step $\tau = 1/80$ K, which determines the number of beads as $M = \frac{\beta}{\tau}$ for a given inverse temperature β . If no off-diagonal operators such as the one-body density matrix need to be averaged, we can set $\mathbf{R}_M = \mathbf{R}_0$. Thus all polymers are closed loops, one for each quantum particle.

We need to account for the indistinguishability of quantum particles. Bose statistics is implemented by symmetrization of the density matrix

$$\rho_B(\mathbf{R}, \mathbf{R}; \beta) = \frac{1}{N!} \sum_P \rho(\mathbf{R}, P\mathbf{R}; \beta) \quad (\text{S2})$$

where the sum is over all permutations P . As can be seen from the right hand side of Eq. (S2), the symmetrization corresponds to reconnecting the imaginary time paths to form larger polymers. For a detailed review of the PIMC method for bosons see Ref. [36], for the application to dopants in ^4He clusters see Refs. [19, 40].

In addition to static quantities, PIMC allows in principle also to calculate dynamical properties. It is straightforward to calculate correlation functions $\langle \hat{A}(t)\hat{A}(0) \rangle$, that are related to measurable spectra via the fluctuation-dissipation theorem. However, PIMC provides these correlation functions only in imaginary time. The analytic continuation of imaginary time data with statistical noise due to finite sampling time to real time is an ill-posed problem. In the present case, we are interested in the rotational spectrum of a linear molecule, which can be obtained from

$$F_\ell(t) = \frac{4\pi}{2\ell+1} \frac{1}{Z} \sum_m \text{Tr}[Y_{\ell m}^+(t) Y_{\ell m}(0) e^{-\beta \hat{H}}]$$

where $Y_{\ell m}$ are spherical harmonics. The spectrum $S_\ell(\omega)$ of rotational excitations $J \rightarrow J + \ell$ (where $\ell = 2$ in the case of a homo-nuclear linear rotor) can be obtained by inverting the Laplace transform, $F_\ell(t) = \int_{-\infty}^{\infty} d\omega e^{-t\omega} S_\ell(\omega)$. Since the inversion is an ill-posed problem, it can only be done approximately and only if the error bars of $F_\ell(t)$ are very small. Therefore, we opted to simply fit the known solution $F_\ell^0(t)$ for a free linear rotor,

$$F_\ell(t) = \frac{4\pi}{2\ell+1} \frac{3}{Z} \sum_{\ell_1, \ell_2} \frac{(2\ell_1+1)(2\ell_2+1)}{4\pi} \begin{pmatrix} \ell_1 & \ell & \ell_2 \\ 0 & 0 & 0 \end{pmatrix}^2 e^{-(\beta-t)B\ell_2(\ell_2+1)} e^{-tB\ell_1(\ell_1+1)}$$

to correlation function $F_\ell(t)$ obtained with PIMC for I_2 in helium with B acting as fit parameter. This fit yields an effective $B = B_{\text{eff}}$, under the assumption that the rotational spectrum of I_2 in helium is essentially that of a linear rotor with a renormalized rotational constant. For heavy rotors this assumption has been validated by experiments. Although the effective distortion constant D_{eff} usually increases by orders of magnitude in helium compared to the gas phase value, D_{eff} is still small and, therefore, we cannot determine it from an improved fit to a free linear rotor with distortion constant D as second parameter.

PIMC simulations of droplets of 10^3 or 10^4 ^4He atoms, as produced in the experiments, would be very demanding. Instead we performed two kinds of simulations of I_2 in helium, that bracket the experimental situation from both sides: I_2 in ^4He clusters of $N = 150$ atoms, much smaller than in experiment; and I_2 in bulk ^4He . Bulk simulations are realized with periodic boundary conditions. 511 ^4He atoms and one I_2 are put in a simulation box of side length

$L = 28.6\text{\AA}$. L is determined by the condition that the ^4He density in the molecule frame of reference, $\rho(r, \theta)$, approaches the equilibrium density of bulk ^4He , $\rho_{eq} = 0.02186\text{\AA}^{-3}$, for large distance r between ^4He atoms and molecule. The largest distance compatible with periodic boundaries is $L/2$, which is large enough to obtain a ^4He density $\rho(r, \theta)$ that fluctuates only slightly around ρ_{eq} . Therefore, we believe that simulations for this size provide a good approximation to the bulk limit. Simulations of I_2 in ^4He cluster were done at a temperature of $T = 0.31\text{K}$, typical for ^4He droplets in equilibrium. For simulations of I_2 in bulk helium, approximated by 511 ^4He atoms, we doubled the temperature to $T = 0.62\text{K}$, in order to reduce the computational demands by cutting the number of beads in half. From the bulk simulations we obtained a ratio of $B_{\text{eff}}/B = 0.60$, while simulations of I_2 in a cluster of $N = 150$ ^4He atoms gave a very similar value of $B_{\text{eff}}/B = 0.58$. We note that for I_2 the ratio B_{eff}/B is large compared to values found for other heavy linear rotors in helium. This smaller relative reduction is due to the particularly large moment of inertia I of I_2 already in the gas phase. A significant *relative* increase of I , and thus significant *relative* reduction of B requires, therefore, a much larger effect of the helium environment than, e.g., for the well-studied OCS molecule in helium, with a moment of inertia more than five times smaller.

The angulon theory

The angulon Hamiltonian

The theoretical approach used here is based on the recently-developed angulon theory [10–15, 22, 41]. We start from the angulon Hamiltonian, which describes a rotating molecule coupled to a bosonic bath [10]:

$$\hat{H} = B\hat{\mathbf{J}}^2 + \sum_{k\lambda\mu} \omega_k \hat{b}_{k\lambda\mu}^\dagger \hat{b}_{k\lambda\mu} + \sum_{k\lambda\mu} U_\lambda(k) [Y_{\lambda\mu}^*(\hat{\theta}, \hat{\phi}) \hat{b}_{k\lambda\mu}^\dagger + Y_{\lambda\mu}(\hat{\theta}, \hat{\phi}) \hat{b}_{k\lambda\mu}], \quad (\text{S3})$$

where we used the notation $\sum_k \equiv \int dk$, and set $\hbar \equiv 1$. The first term of Eq. (S3) corresponds to the rotational kinetic energy of a linear-rotor molecule, with $\hat{\mathbf{J}}$ the angular momentum operator and $B = 1/(2I)$ the molecular rotational constant, where I is the molecular moment of inertia. The bare eigenstates of the molecular impurity are given by the $(2L + 1)$ -fold degenerate states, $|L, M\rangle$, with energies $E_L = BL(L + 1)$. Here L is the angular momentum quantum number, and M is its projection on the laboratory-frame z -axis.

The second term of Eq. (S3) gives the kinetic energy of the superfluid excitations, such as phonons and rotons, whose spectrum is described by the dispersion relation ω_k . Here, the operators $\hat{b}_{k\lambda\mu}^\dagger$ ($\hat{b}_{k\lambda\mu}$) are creating (annihilating) a superfluid excitation with linear momentum $k = |\mathbf{k}|$, the angular momentum λ , and its projection, μ , onto the z -axis. These operators can be obtained using the spherical-harmonic expansion of the usual creation/annihilation operators in Cartesian space, $\hat{b}_{\mathbf{k}}^\dagger$ and $\hat{b}_{\mathbf{k}}$, see Refs. [10–12] for details.

The last term of the Hamiltonian (S3) describes the angular-momentum exchange between the molecular impurity and the superfluid, where the coupling constants $U_\lambda(k)$ are proportional to the Legendre moments of the molecule–Helium potential energy surface in Fourier space. Here $Y_{\lambda\mu}(\hat{\theta}, \hat{\phi})$ are spherical harmonics [42], which depend on the molecular angle operators in the laboratory frame, $(\hat{\theta}, \hat{\phi})$. This type of coupling, explicitly dependent on the three-dimensional impurity orientation, makes Eq. (S3) substantially different from other impurity problems such as, e.g., the Bose-polaron [43] or the spin-boson [44] models.

Originally, the Hamiltonian (S3) was derived to describe an ultracold molecule interacting with a dilute BEC, where the coupling constants $U_\lambda(k)$ assume a simple analytic form [10, 11]. Helium, on the other hand, represents a dense, strongly-interacting superfluid, which makes it quite challenging to derive the coupling constants from first principles.

However, by analogy with effective field theories of nuclear [45] and condensed matter [46] physics, the angulon Hamiltonian (S3) can be approached from a phenomenological perspective, where the effective low-energy constants are extracted from experiment or *ab initio* calculations. As an example, recently it was shown that the effective rotational constants of 25 different molecules in superfluid helium can be obtained from the angulon theory in good agreement with experiment, based on only two phenomenological parameters [22]. Here we pursue a similar approach to calculate the dynamical properties of the I_2 molecule in helium.

Effective rotational constants

Interactions of a heavy molecule, such as I_2 , with helium can be most naturally understood if one rewrites the Hamiltonian (S3) in the rotating molecular frame [22]. This is achieved by applying a canonical transformation

recently introduced by Schmidt and Lemesko [12]:

$$\hat{S} = e^{-i\hat{\phi}\otimes\hat{\Lambda}_z} e^{-i\hat{\theta}\otimes\hat{\Lambda}_y} e^{-i\hat{\gamma}\otimes\hat{\Lambda}_z}. \quad (\text{S4})$$

Here $(\hat{\phi}, \hat{\theta}, \hat{\gamma})$ are the angle operators which act in the Hilbert space of the molecular rotor, and

$$\hat{\Lambda} = \sum_{k\lambda\mu\nu} \hat{b}_{k\lambda\mu}^\dagger \sigma_{\mu\nu}^\lambda \hat{b}_{k\lambda\nu} \quad (\text{S5})$$

is the total angular momentum operator of the superfluid excitations, acting in their corresponding Hilbert space. The angular momentum matrices, $\sigma^\lambda \equiv \{\sigma_{-1}^\lambda, \sigma_0^\lambda, \sigma_{+1}^\lambda\}$, fulfill the $SO(3)$ algebra in the representation of angular momentum λ . Thus, the transformation of Eq. (S4) transfers the superfluid degrees of freedom into the rotating molecular frame.

The transformed Hamiltonian assumes the following form:

$$\hat{\mathcal{H}} \equiv \hat{S}^{-1} \hat{H} \hat{S} = B(\hat{\mathbf{L}} - \hat{\Lambda})^2 + \sum_{k\lambda\mu} \omega_k \hat{b}_{k\lambda\mu}^\dagger \hat{b}_{k\lambda\mu} + \sum_{k\lambda} \tilde{U}_\lambda(k) [\hat{b}_{k\lambda 0}^\dagger + \hat{b}_{k\lambda 0}] \quad (\text{S6})$$

where $\tilde{U}_\lambda(k) = \sqrt{(2\lambda+1)/(4\pi)} U_\lambda(k)$. The operator $\hat{\mathbf{L}} \equiv \hat{\mathbf{J}} + \hat{\Lambda}$ is the *total* angular momentum operator, which acts in the molecular Hilbert space. The components of $\hat{\mathbf{L}}$ define projections of total angular momentum in the rotating molecular frame and, therefore, obey anomalous commutation relations [47, 48]. In the absence of external fields, total angular momentum $\hat{\mathbf{L}}$ is conserved, which allows to solve the problem for each value of L separately.

Another advantage of the transformed Hamiltonian (S6) is that it can be diagonalized exactly in the limit of a slowly rotating molecule, $B \rightarrow 0$. There, for each total angular momentum state, $|LM\rangle$, the ground state is given by:

$$|\psi_{LM}\rangle = e^{\sum_{k\lambda} \frac{\tilde{U}_\lambda(k)}{\omega_k} (\hat{b}_{k\lambda 0} - \hat{b}_{k\lambda 0}^\dagger)} |0\rangle |LM\rangle. \quad (\text{S7})$$

Note that the bosonic coherent state of Eq. (S7) involves an infinite number of superfluid excitations and, therefore, describes a collective anisotropic displacement of helium atoms. Such a deformation can be thought of as a microscopic formulation of the ‘nonsuperfluid helium shell’ which rotates along with the molecule [1, 3].

It is important to note that the angulon theory based on the transformed Hamiltonian, Eq. (S6), provides a simple physical explanation for renormalization of molecular rotational constants in superfluid helium. The rotational energy of the molecular impurity is defined by the first term of Eq. (S6), while the rest of terms ultimately determine how many phonons are excited due to the molecule-helium interactions. In the absence of helium, the total angular momentum is given by that of a free molecule, $\hat{\mathbf{L}} \equiv \hat{\mathbf{J}}$. In the presence of helium, $\hat{\mathbf{L}}$ is still a conserved quantity, however, the stronger the molecule-helium interactions the larger is the angular momentum of the superfluid, $\hat{\Lambda}$. Thus, for a given *total* angular momentum L , the rotational energy is lower in the presence of helium ($\hat{\Lambda} \neq 0$) compared to a gas-phase molecule ($\hat{\Lambda} = 0$), which leads to renormalization of the molecular rotational constant.

In our approach, we calculate the amount of the angular momentum transferred to the superfluid for the state of Eq. (S7):

$$\langle \hat{\Lambda}^2 \rangle \equiv \langle \psi_{LM} | \hat{\Lambda}^2 | \psi_{LM} \rangle = \sum_{k\lambda} \lambda(\lambda+1) \frac{\tilde{U}_\lambda^2(k)}{\omega_k^2}, \quad (\text{S8})$$

and replace the boson angular momentum operator in Eq. (S6) by its expectation value, $\hat{\Lambda} \rightarrow \langle \Lambda \rangle \equiv \langle \hat{\Lambda}^2 \rangle^{1/2}$. Then, assuming that $\hat{\Lambda}$ points along the total angular momentum, $\hat{\Lambda} \sim \hat{\mathbf{L}}$, we can evaluate the effective rotational constant as:

$$B_{\text{eff}} = B(1 - \beta)^2, \quad (\text{S9})$$

where

$$\beta = \left(\frac{1}{2} \sum_{k,\lambda} \lambda(\lambda+1) \frac{\tilde{U}_\lambda(k)^2}{\omega_k^2} \right)^{1/2}. \quad (\text{S10})$$

Within our approach, we treat β as a phenomenological parameter and set it to $\beta = 0.23$, which reproduces the results of quantum Monte Carlo calculations giving $B_{\text{eff}} = 0.6B$. In addition, Eq. (S10) enables us to calculate the α_2 parameter as discussed below.

Dynamics of I₂ in helium

We perform the calculations of the time evolution in the laboratory frame, as given by the Hamiltonian (S3), with B replaced by $B_{\text{eff}} = 0.6 B_0$, as discussed above. Since the pulse is very short, $\tau \ll B^{-1}, U_\lambda(k)^{-1}, \omega_k^{-1}$, the state after the pulse can be found within the impulsive approximation [49]. To this end, we assume that the interaction with the laser pulse is described by the potential

$$\hat{V}(t) = -\eta \delta(t) \cos^2 \hat{\theta}. \quad (\text{S11})$$

Here, η is a dimensionless parameter related to the fluence of the kick pulse. The laser fluences presented in Fig. 1(a)–(e) correspond to the values of $\eta = 2.6, 5.2, 13, 26$, and 39 , respectively. The subsequent time evolution of the wave function is given by:

$$|\psi(t)\rangle = e^{-i\hat{H}t} e^{\eta \cos^2 \hat{\theta}} |\psi_0\rangle. \quad (\text{S12})$$

Before the laser pulse, the He-dressed molecular states in the laboratory frame are obtained by applying an inverse transformation of Eq. (S4) to Eq. (S7), which results in:

$$|\psi_0\rangle = e^{\sum_{k\lambda\mu} \frac{\tilde{U}_\lambda(k)}{\omega_k} (\hat{b}_{k\lambda\mu} Y_{\lambda\mu}(\hat{\Omega}) - \hat{b}_{k\lambda\mu}^\dagger Y_{\lambda\mu}^*(\hat{\Omega}))} |j_0, m_0\rangle_{\text{mol}} \otimes |0\rangle_{\text{b}}, \quad (\text{S13})$$

where $\hat{\Omega} \equiv (\hat{\theta}, \hat{\phi})$ and $|0\rangle_{\text{b}}$ is the bosonic vacuum state. Since after the pulse the wave function represents a superposition of rotational energy levels, the time-evolution of the angulon state is given by:

$$|\psi(t)\rangle = e^{-i\hat{H}t} \sum_j c_j e^{\sum_{k\lambda\mu} \frac{\tilde{U}_\lambda(k)}{\omega_k} (\hat{b}_{k\lambda\mu} Y_{\lambda\mu}(\hat{\Omega}) - \hat{b}_{k\lambda\mu}^\dagger Y_{\lambda\mu}^*(\hat{\Omega}))} |j, m_0\rangle_{\text{mol}} \otimes |0\rangle_{\text{b}}, \quad (\text{S14})$$

where the coefficients c_j depend on j_0 , m_0 , and η . For the wave function (S14), we calculate the evolution of the molecular alignment as

$$\langle \cos^2 \theta_{2D} \rangle(t) \equiv \langle \psi(t) | \cos^2 \hat{\theta}_{2D} | \psi(t) \rangle, \quad (\text{S15})$$

where $\cos^2 \hat{\theta}_{2D} \equiv \cos^2 \hat{\theta} / (\cos^2 \hat{\theta} + \sin^2 \hat{\theta} \sin^2 \hat{\phi})$ is a two-dimensional projection of the three-dimensional alignment cosine, $\cos^2 \hat{\theta}$, as measured in the experiments.

Performing the time evolution of the considered wave function using Eqs. (S3) and (S14) is an involved many-particle problem because the interaction term of the Hamiltonian does not commute with the rest of the terms. First of all, we note that the boson kinetic energy can be eliminated by rewriting the Hamiltonian in the rotating frame, which corresponds to the replacements $\hat{b}_{k\lambda\mu}^\dagger \rightarrow \hat{b}_{k\lambda\mu}^\dagger e^{-i\omega_k t}$, $\hat{b}_{k\lambda\mu} \rightarrow \hat{b}_{k\lambda\mu} e^{i\omega_k t}$. Since in the final expression for the alignment cosine the oscillating exponents cancel with their corresponding complex conjugates, the boson kinetic energy contributes only through the initial state, Eq. (S13). In order to account for the rest of the Hamiltonian, we apply an expansion of the Suzuki-Trotter type:

$$e^{-it\hat{H}} \approx e^{-itB\hat{\mathbf{J}}^2/2} e^{-it\sum_{k\lambda\mu} U_\lambda(k) [Y_{\lambda\mu}^*(\hat{\theta}, \hat{\phi}) \hat{b}_{k\lambda\mu}^\dagger + Y_{\lambda\mu}(\hat{\theta}, \hat{\phi}) \hat{b}_{k\lambda\mu}]} e^{-itB\hat{\mathbf{J}}^2/2}, \quad (\text{S16})$$

which becomes exact in the limit of small t . Furthermore, in order to decrease the number of free parameters of the model, we take into account only the leading anisotropic term, $\lambda = 2$, of the He-I₂ PES [20, 22]. The resulting alignment cosine can be derived in closed form:

$$\begin{aligned} \langle \cos^2 \hat{\theta}_{2D} \rangle(t) &= \sum_{j, j', j_1, j_2, m} c_{j'}^* c_j e^{it(E_{j_2} + E_{j'} - E_{j_1} - E_j)/2} \langle j_2 m | \cos^2 \hat{\theta}_{2D} | j_1 m \rangle \\ &\times \int d\Omega_1 \int d\Omega_2 Y_{j'm_0}^*(\Omega_2) Y_{j_2 m}(\Omega_2) Y_{j m_0}(\Omega_1) Y_{j_1 m}^*(\Omega_1) e^{(\alpha_1 t^2 + \alpha_2) [\frac{4\pi}{5} \sum_\mu Y_{2,\mu}(\Omega_2) Y_{2,\mu}^*(\Omega_1) - 1]}, \end{aligned} \quad (\text{S17})$$

where $\int d\Omega \equiv \int \sin \theta d\theta d\phi$ and we have defined

$$\alpha_1 \equiv \sum_k U_2^2(k), \quad \alpha_2 \equiv \sum_k \frac{U_2^2(k)}{\omega_k^2}. \quad (\text{S18})$$

The α_1 parameter determines the decay rate of the alignment. We take $\alpha_1 = 10$ (in units of $1/B_{\text{eff}}^2$), which reproduces the decay rate observed in experiment for $F_{\text{kick}} = 1.2 \text{ J/cm}^2$. The α_2 parameter can be determined using Eq.(S8) and the value of $B_{\text{eff}} = 0.6B_0$ and turns out to be very small $\alpha_2 \approx 0.04$. Previous experiments on microwave spectroscopy of molecules in helium droplets have shown a broadening of the molecular rotational lines, which amounts to $\sim 100 \text{ MHz}$ in the case of OCS [2]. The line shapes are attributed to inhomogeneous broadening, and at least for CO in helium this was confirmed by calculations [50]. In order to account for this effect, we introduce a Gaussian broadening of B_{eff} values with a standard deviation $\gamma = 0.05 B_{\text{eff}}$, which corresponds to half width at half maximum of 66 MHz for I_2 . Explicitly, we use the energy levels $E_j \equiv (B_{\text{eff}} + \gamma x)j(j+1)$, where x is drawn from a normal distribution and we integrate the result for $\langle \cos^2 \theta_{2D} \rangle(t)$ over x .

In addition, we calculate the survival probability of the initial state as:

$$S(t) = \left| \sum_j |c_j|^2 e^{-itE_j} \right|^2 e^{-\alpha_1 t^2}. \quad (\text{S19})$$

Ensemble averaging: temperature and symmetry

Since the temperature of He droplets, $T = 0.38 \text{ K}$, is larger than the rotational constant $B_{\text{eff}} = 0.032 \text{ K}$, one needs to account for the thermal distribution of population over several rotational states, as given by the Boltzmann distribution:

$$P_j = Z^{-1} e^{-B_{\text{eff}}j(j+1)/(k_B T)}. \quad (\text{S20})$$

where k_B is the Boltzmann constant and $Z \equiv \sum_j P_j$ is the partition function. For the temperature stated above, it is sufficient to truncate the sum at $j = 6$, which corresponds to 28 lowest $|jm\rangle$ -levels.

In addition to the thermal distribution, we account for the 21 : 15 ortho-to-para ratio of I_2 . This corresponds to an averaging over molecules in even and odd rotational states:

$$P_j^{\text{even}} = Z_{\text{even}}^{-1} e^{-B_{\text{eff}}j(j+1)/(k_B T)}, \quad (\text{S21})$$

$$P_j^{\text{odd}} = Z_{\text{odd}}^{-1} e^{-B_{\text{eff}}[j(j+1)-2]/(k_B T)}, \quad (\text{S22})$$

where the reference energy for odd states is $2B_{\text{eff}}$ – the rotational energy of the lowest odd state with $j = 1$. The corresponding partition functions are given by $Z_{\text{even(odd)}} \equiv \sum_{j \in \text{even(odd)}} P_j^{\text{even(odd)}}$. The thermally-averaged result for the alignment, $a(t)$, of the odd and even states is given by:

$$\langle \cos^2 \theta_{2D} \rangle_{\text{even(odd)}}(t) = \sum_{j_0 \in \text{even(odd)}, m_0} \langle \psi(t) | \cos^2 \theta_{(2D)} | \psi(t) \rangle^{(j_0, m_0)} \times P_j^{\text{even(odd)}}, \quad (\text{S23})$$

where the (j_0, m_0) superscript denotes alignment with the starting $|j_0, m_0\rangle$ state of the molecule. Finally, the ensemble-averaged result is obtained as

$$\langle \cos^2 \theta_{2D} \rangle(t) = \frac{15 \times \langle \cos^2 \theta_{2D} \rangle_{\text{even}}(t) + 21 \times \langle \cos^2 \theta_{2D} \rangle_{\text{odd}}(t)}{15 + 21}. \quad (\text{S24})$$

Eq. (S24) was the one we used to compare the theory to experiment.